OPTIMIZATION OF PHOTONIC CRYSTAL ENHANCED FLUORESCENCE BY EXCITATION LASER ANGLE SCANNING

BY

VIKRAM CHAUDHERY

THESIS

Submitted in partial fulfillment of the requirements
for the degree of Master of Science in Electrical and Computer Engineering
in the Graduate College of the
University of Illinois at Urbana-Champaign, 2011

Urbana, Illinois

Adviser:

Professor Brian T. Cunningham

ABSTRACT

Photonic crystal enhanced fluorescence (PCEF) has been demonstrated as an effective means for amplifying the excitation provided to surface-bound fluorescent molecules while simultaneously enhancing fluorescence emission collection efficiency. Optimal coupling of a fluorophore-exciting light source to the PC occurs with the use of collimated plane waves, as utilized in a special-purpose fluorescence microscope specifically designed for coupling with PCEF surfaces. However, PCEF surfaces are also capable of coupling light from focused sources, such as those used in commercially available confocal laser scanners, but with a reduction in the obtainable enhancement factor. Using computer simulations and experimental measurements, we describe the interaction between the resonant bandwidth of a PCEF device surface and the optical design of the detection instrumentation that is used to provide fluorescence excitation. We show that highly collimated illumination is required for achieving the greatest PCEF enhancement factors, but at the expense of poor tolerance to nonuniformities in resonant wavelength across the PCEF surface. To overcome this limitation, we demonstrate a fixed wavelength/multiple incident angle scanning detection system that is capable of measuring every pixel in a PCEF fluorescence image under conditions that optimize resonant excitation efficiency. Finally we discuss the enhanced excitation mechanism for photonic crystal enhanced fluorescence in the context of photobleaching. We show that the photobleaching rate of dye molecules on the photonic crystal surface is accelerated by 30x compared to an ordinary glass surface, but substantial signal gain is still evident, even after extended periods of continuous illumination at the resonant condition.

ACKNOWLEDGMENTS

This work would not have been possible without the continued support and insight of my adviser, Professor Brian Cunningham. I also wish to acknowledge several past and present members of the Nano Sensors Research Group for our many fruitful discussions: Meng Lu, Erich Lidstone, Cheng-Sheng Huang, Anusha Pokhriyal, Sherine George, Patrick Mathias, and Ian Block. I would also like to thank the support staff at the Micro and Nanotechnology Laboratory at the University of Illinois. Gratitude is also due to Professor Gabriel Popescu and Dr. Peter Dragic for their valuable guidance and discussions, both at the University of Illinois. Finally, I would like to thank my family and friends for their support and encouragement throughout my academic career.

I also gratefully acknowledge the National Science Foundation, U.S. Army and SRU Biosystems for providing financial support for this work.

TABLE OF CONTENTS

CHAPTER 1: INTRODUCTION

Fluorescence has emerged as a useful tool for imaging and detection in medical and biological sciences due to its excellent sensitivity, the wide availability of dye molecules, ease of application to broad classes of biomolecules, and robust detection instrumentation. The major limitation of fluorescence is the signal strength, which in turn can often limit visualization and quantification of low concentration analytes in numerous fluorescence based assays [1, 2]. To address the need for higher sensitivity and improved signal-to-noise ratio (SNR) in surface-based fluorescence assays, dielectric-based photonic crystal (PC) surfaces have been utilized in the context of gene expression analysis [3] and protein biomarker detection [4].

PC surfaces provide a consistent and highly efficient platform for enhancement of fluorescence. Their optical resonance characteristics can be exploited to provide not only a heightened excitation field (resulting in a phenomenon called “enhanced excitation”), but also control over the photonic dispersion, providing a powerful mechanism to redirect the emitted light into certain preferred directions, where it can be detected with greater efficiency (“enhanced extraction”). The simultaneous implementation of these two techniques has been shown to boost the radiation detected from quantum dots and fluorescent dye molecules by two orders of magnitude [5-8].

Enhanced excitation results from high energy density electromagnetic fields on the surface of the PC at resonance. For a given PC structure, the resonance modes have a distinct coupling angle and wavelength combination [9, 10]. Externally, the guided-mode resonance is observed as an efficient reflection peak (~100% reflection) over a narrow range of incident angles for illumination at a given wavelength, thus acting like an optical filter [11, 12]. Physically, the

leaky resonances of the PC are excited by an external light source, such as a laser. As the excited leaky modes are localized in space during their finite lifetimes, they can be engineered to have very high energy density within regions of the PC at resonance. The magnitude of this energy density is directly related to the resonant mode lifetime, or Q-factor, which in turn can be controlled by adjusting the device parameters. (Q is mathematically defined as $\lambda/\Delta\lambda$, where λ is the resonant wavelength, and $\Delta\lambda$ is the full width at half maximum of the resonant peak spectrum.) The intensity of fluorophore emission (which is absorptive at the resonant wavelength) can be greatly enhanced by placing dye molecules in proximity to regions where the resonant modes concentrate most of their energy. To produce a stronger resonant field, it is important to use a high-Q PC cavity [13], resulting in a narrow range of angles that couple to the PC for a given wavelength. Therefore, a narrow beam divergence is necessary to efficiently couple a laser to the modes of a PC enhanced fluorescence (PCEF) surface. The PC physical design parameters are used to intentionally provide a desired Q-factor, and the achievable enhanced excitation effect scales with Q.

Enhanced extraction is also possible due to the availability of rich and highly flexible photonic band dispersion, opening up the possibility for engineering the far-field fluorescent emission pattern [14]. When fluorescent species are placed on the PC surface and emit radiation that is able to couple to the photonic dispersion, the result is a powerful mechanism to redirect the emitted light into certain preferred directions, where it can be detected with greater efficiency. Such a scheme further enables efficient collection of the emitted radiation and, therefore, lower detection limits.

While the effects of PC enhanced excitation and enhanced extraction can be combined with multiplicative effects [5, 7, 8], this work is primarily concerned with optimization of enhanced

excitation through the interaction of the PC resonant mode characteristics and the degree of collimation of the illumination that is provided to the PC.

In previous work, a confocal laser scanner, incorporating a focused laser beam, was used to good effect for PCEF [5, 15]. However, due to the angle selectivity of the PCEF surface, only a portion of the excitation energy can be coupled into the resonance mode and contribute to enhanced fluorescence emission. To improve PCEF performance, we demonstrated the use of a collimated excitation scheme [7], in which the excitation beam matches the resonance angle of the target resonance mode. In the detection instrument described in previous work, a single excitation angle (at a fixed illumination wavelength) was selected for imaging an entire PC surface. Using this fixed angle/fixed wavelength excitation approach, only limited regions of a high-Q PCEF surface could be optimally excited. While some parts of the PC were precisely "on-resonance" and therefore experienced the greatest enhancement factor, small variations in fabrication parameters or surface chemistry density would result in regions of the PC that were not optimally resonant with the excitation source, resulting in lower enhancement factor. Fundamentally, this effect occurs because small changes in optical density on the PC surface result in a shift in reflected wavelength (for a fixed illumination angle) – an effect that has been used effectively for PC-based label-free detection [16-24]. When considering the use of PCEF surfaces for multiplexed assays using an array of immobilized biomolecule capture spots, this problem is especially critical because the optical density associated with the capture molecules substantially modifies the resonant conditions on the PCEF surface. This phenomenon results in a situation in which the conditions for optimal enhanced excitation can be substantially different from spot to spot within a microarray.

This study begins by characterizing the field enhancement capability of PCEF surfaces excited by laser beams with different degrees of divergence. A numerical scheme is derived to evaluate the field enhancement factor of PCEF surfaces in Chapter 2. The results quantify how the fluorescence signal enhancement on the PCEF surface directly benefits from using a collimated excitation beam, and confirm that optimal coupling for enhanced excitation occurs for only a narrow range of incident angles for a fixed excitation wavelength. Focused illumination is shown to also provide effective enhanced excitation with a lower enhancement factor than collimated illumination, while providing greater tolerance to variation of the PC. The results also show that the Q-factor of the resonance can be effectively controlled through modulation of the PC grating depth. In Section 4.2, these effects are demonstrated experimentally through characterization of a PCEF surface with deposited spots of dye-labeled peptides. Collimated illumination is used to obtain enhancement factors of over 600x while an enhancement factor of only 30x is measured on the same device using a commercially available confocal laser scanner. Section 4.3 presents a solution to the fundamental problem of PC surface optical density uniformity by implementing a novel approach that gathers fluorescent images for a range of angles, scanned in small increments. Software is able to select the optimal resonant coupling angle on a pixel-by-pixel basis to construct a fluorescent image in which every region on the PC surface is measured with the highest possible enhancement factor. The method was applied to a 1×3 in^2 PCEF surface. This technique, while beneficial to uniform signal enhancement, may result in photobleaching of the dye molecules due to continuous exposure to excitation laser light. Chapter 5 addresses the effect of photobleaching in PCs with the goal of understanding and quantifying the extent to which photobleaching may affect fluorescence signal output of dye-labeled peptides.

CHAPTER 2: COUPLING OF PC SENSOR AND EXCITATION LIGHT

The PC is a periodic arrangement of dielectric materials with sub-wavelength period, where the device reflects ~100% of the incident light at a specific wavelength and a specific angle. The wavelength and angle that match the coupling condition are defined as the resonant wavelength (λ_r) and the resonant angle (θ_r). When the coupling conditions are satisfied, the resonant mode confined near the sensor surface is excited, and exhibits amplified field intensity, which enhances the fluorescent dye emission immobilized within a 200 nm region above the PC surface [25]. Unlike evanescent coupled optical micro- or nano-resonators [26, 27], which require highly precise position control, input light is coupled into PC resonator mode via angle and wavelength control. When most of the excitation beam is coupled into resonant mode, the near field strength becomes strong and consequently the PC sensor provides fluorescence enhancement. However, in the case of weak coupling, the PC enhancement effect is substantially diminished. A laser (He-Ne, λ=632.8 nm) is used to excite a specific fluorophore in the study. Therefore, the resonant wavelength of the PC surface was designed to overlap with the laser emission wavelength by tuning the angle of incidence.

2.1 Photonic Crystal Sensor Design

Figure 2.1 shows a schematic model of the PC structure, which is comprised of a quartz substrate with the top surface etched to provide a periodic refractive index modulation. On top of the grating, a high refractive index thin film of titanium oxide (TiO_2) is deposited as a wave guidance layer. The introduced periodic modulation allows for phase-matching of an external incident beam into leaky resonant modes that can be re-radiated into free space [6, 28]. The λ_r,

θ_r, and bandwidth of the resonant mode can be controlled through proper selection of the grating period (Λ), grating depth (d), and thickness of the high index layer (t) depicted in Figure 2.1 [29].

The goal of designing the PC surface for fluorescence enhancement is to produce a strongly enhanced near field. A high Q-factor (i.e. narrow bandwidth) PC structure is desirable to improve near field intensity [25]. In a 1D PC structure, the major contributor to energy loss is out-of-plane scattering by the grating structure. To improve cavity Q-factor and to enhance near field intensity, a PC structure with smaller index modulation strength is desirable. Shallower grating depth reduces the out of surface coupling and significantly improves Q-factor. To examine the relationship between Q-factor and grating depth, an RCWA software package (Diffract MOD, RSOFT Design) was used to calculate the transmission efficiency as a function of illumination angle. An incident beam of λ_r and θ_r can be coupled into a resonant mode, resulting in a dip in the transmission efficiency, as measured in the far field. PC structures with three different grating depths (15 nm, 30 nm, and 100 nm) were studied. For all three PC structures, the grating period is Λ=400 nm while the TiO_2 thickness was selected to maintain a resonant angle of 10° at a resonant wavelength of 633 nm (t_{TiO} = 155 nm, 158 nm and 185 nm). The angle transmission spectra are shown in Figure 2.2. As expected, using shallower grating depth increases the Q-factor. However, as the Q-factor increases, the coupling condition becomes more stringent. For example, the angle tolerance of a d=100 nm grating is 0.76°, but the angle acceptable range of a d=15 nm grating is only 0.06°. In order to fully utilize the field enhancement capability of high Q-factor PC surfaces, the illumination must be well collimated.

2.2 Resonant Field Distribution for Diverged Beam Excitation

Unfocused laser beams are highly collimated, but exhibit divergence that results in incident angle components with a Gaussian distribution around normal. It is particularly important to note that commercially available fluorescence laser scanners use a focused laser beam [30-32]. As we move towards higher Q-factors for PCEF, the angle tolerance for exciting a resonant mode decreases. Therefore, it is important to consider the beam divergence of the excitation light for optimal performance.

Here we develop a calculation scheme to quantify how beam divergence affects the enhancement factor. A commercially available rigorous coupled wave analysis (RCWA) solver (RSoft DiffractMod) can only output the field distribution in a PC that is excited by a plane wave. To simulate real laser excitation conditions, an analytical approach is combined with RCWA to provide field intensity distribution for a PC surface illuminated by any diverging beam.

The total near field amplitude distribution $\mathbf{E}(\mathrm{x},\mathrm{z})$ is averaged for field distribution at a specific angle θ_j (*j* is an integer number from *0* to *n*) weighted by the intensity of the excitation beam $I(\theta_\mathrm{j})$. The field distribution at an individual angle, $\mathbf{E}_{\theta_\mathrm{j}}(\mathrm{x},\mathrm{z})$, is calculated using RCWA. The expression of $\mathbf{E}(\mathrm{x},\mathrm{z})$ is given by

$$\mathbf{E}(\mathrm{x},\mathrm{z}) = \sum_{\mathrm{j}=0}^{\mathrm{n}} I(\theta_\mathrm{j})\mathbf{E}_{\theta_\mathrm{j}}(\mathrm{x},\mathrm{z}) . \tag{2.1}$$

The spatial intensity distribution of a Gaussian beam propagating along the z-axis is given by

$$\tilde{I}(x,z) = I_0\left[\frac{w_0}{w(z)}\right]^2 e^{-\left(\frac{2x^2}{w^2(z)}\right)}, \tag{2.2}$$

where w_0 and $w(z)$ represent the minimum spot size and spot size at *z*, respectively [33].

In order to find the intensity distribution in terms of angle, the spatial distribution function is transformed into *k*-space governed by $\tilde{I}(x,z) \Leftrightarrow I(\theta,z)$. The expression of the angle dependent intensity distribution function is

$$I(\theta) = I_0\sqrt{\frac{\pi}{2}}\frac{w_0^2}{w(z)}e^{-\frac{1}{2}\left((k_0 sin\theta)^2 \frac{w^2(z)}{8}\right)}. \tag{2.3}$$

After focusing by a lens with a focal length *f*, the angle intensity distribution is given by

$$I(\theta) = I_0' e^{-\frac{1}{2}\left(k_0 sin\theta \frac{\lambda f}{\pi L}\right)^2}, \tag{2.4}$$

where $I_0' = \sqrt{\frac{2}{\pi}}\frac{\lambda f}{L}$ and *L* represents the diameter of the laser beam. In the case of a beam illuminating at the resonant angle, θ_r, Eq. 2.4 can be written as

$$I(\theta - \theta_r) = I_0' e^{-\frac{1}{2}\left[\left(\frac{\lambda}{\pi}\right)^2 F^2 k_0^2 sin^2(\theta-\theta_r)\right]}, \tag{2.5}$$

where $F = f/L$. Substituting Eq. 2.5 into Eq. 2.1, the averaged field amplitude is given by

$$\mathbf{E}(x,z) = \sum_{j=0}^{n} I(\theta_j - \theta_r)\mathbf{E}_{\theta_j}(x,z). \tag{2.6}$$

2.3 Simulation of Field Enhancement Factor

Using the developed numerical methods, we evaluated the field enhancement factor for the PC structures. Since the resonant angle of the PC surfaces are designed for an incident angle of θ=10°, the RCWA was used to calculate field distributions in one period of the PC for 0°<θ<20° with increments of 0.01°. The illumination intensity at a particular angle (θ_j) is calculated using

Eq. 2.5 and multiplied with the field amplitude distribution, $\mathbf{E}_{\theta_j}(x,z)$, which was simulated using RCWA. The averaged field intensity was found by taking the square of $\mathbf{E}(x,z)$. Since the PC enhancement is a near field effect that is localized to the vicinity of sensor surface, only the field intensity within a 50 nm region above the surface is counted. The ratio of the averaged field intensity as compared to the intensity on a reference glass slide is defined as the enhancement factor. Assuming a laser spot with 1 mm diameter, the divergence of the beam after focusing can be altered using a lens with different focal lengths. In the simulation, we consider the laser beam with divergence between 3.3° and 0.00033°. As shown in Figure 2.3, when the excitation beam is highly diverging, the enhancement factor of a low Q-factor PC is higher than that of the high Q-factor PC. However, the high Q-factor PC exhibits an enhancement factor of 263x if the excitation beam becomes more collimated. An excitation beam with angle of divergence beyond 0.005° can be fully coupled into the resonance. An excessively collimated beam will not result in a better enhancement factor once the coupling condition is met.

To further illustrate the field enhancement effect, the averaged near field intensities of gratings with depth d=15 nm were calculated and compared in Figure 2.4 for three exemplary excitation beams with divergence of 11.46°, 0.1146°, and 0.01146°. We investigate the effect of variations in excitation beam divergence on near field strength. In Figure 2.4, the field distribution in a single period of the PC structure is plotted at the resonant wavelength. The white contour highlights the surface of the grating substrate and the top of the PC surface. Figure 2.4(a) demonstrates the field intensity distribution at laser beam divergence of 11.46°. Compared to the mode profile given in Figure 2.4(a), the near field shown in Figure 2.4(b) is ~60 times stronger when the excitation beam is less divergent (0.1146°). For the case of least divergence shown in

Figure 2.4(c), the field intensity is highest (~507 times higher than the least divergent case!). This example illustrates that using a highly collimated excitation source is critical to achieving the greatest enhanced near field.

2.4 Figures

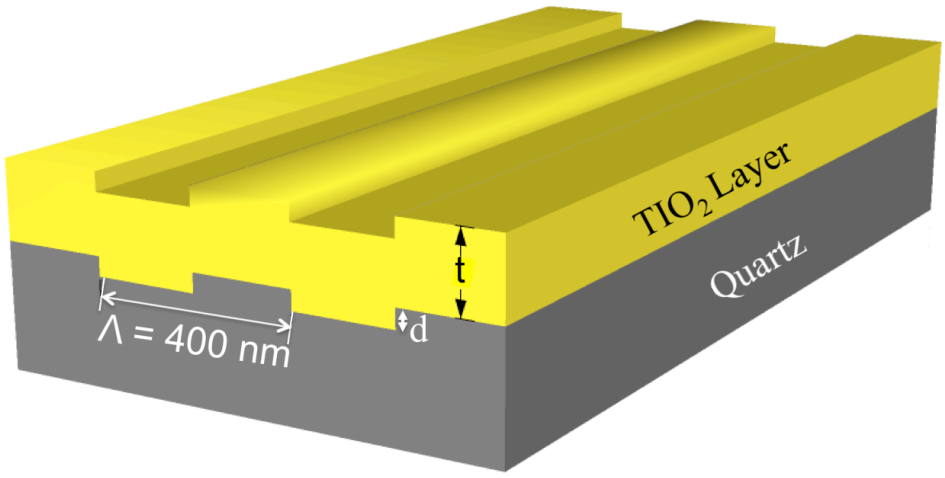

Figure 2.1 Schematic diagram of a PC sensor. The grating structure is etched into a quartz substrate with period and duty cycle of 400 nm and 50%, respectively.

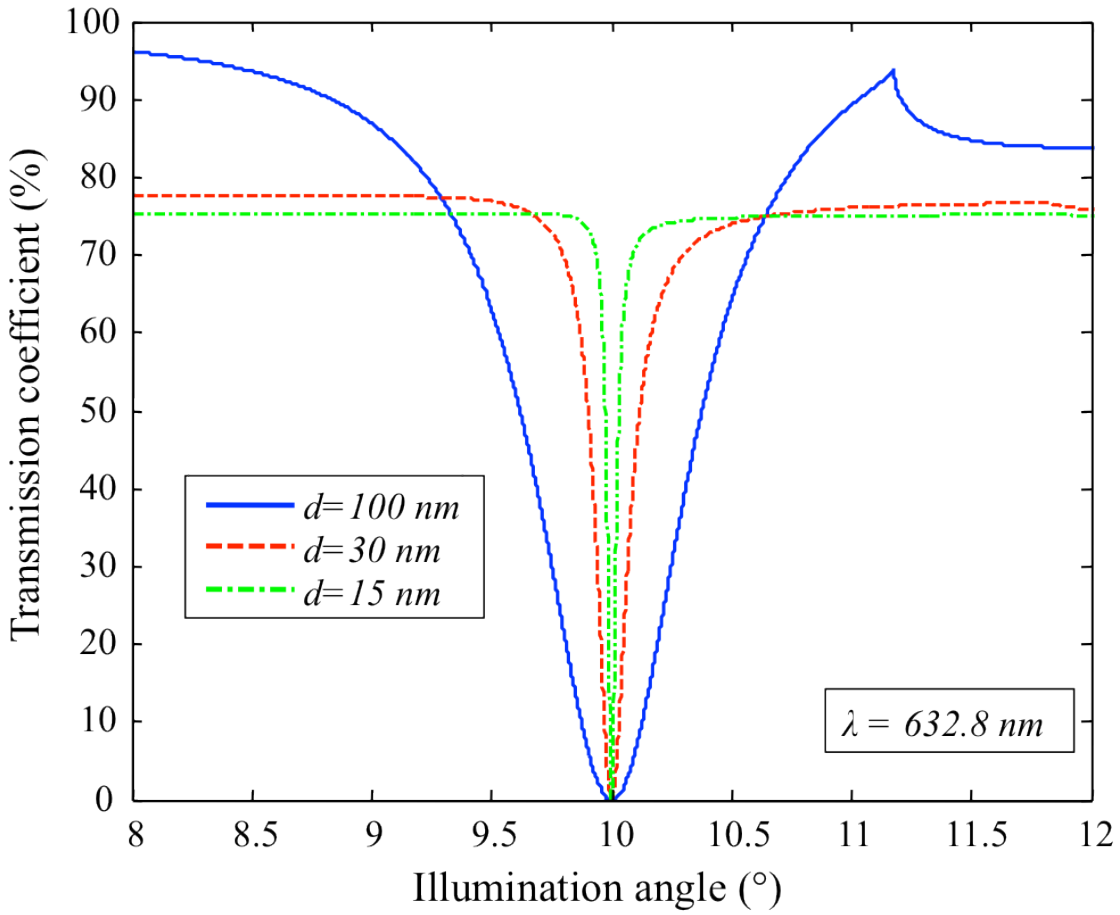

Figure 2.2 Simulated transmission spectra of three different PC designs. The PC gratings have depths of 15 nm, 30 nm, and 100 nm, respectively. The period of the gratings is 400 nm and the TiO_2 thicknesses are 155 nm, 158nm, and 185 nm, respectively, to maintain a constant angle of resonant coupling for a wavelength of λ=632.8 nm.

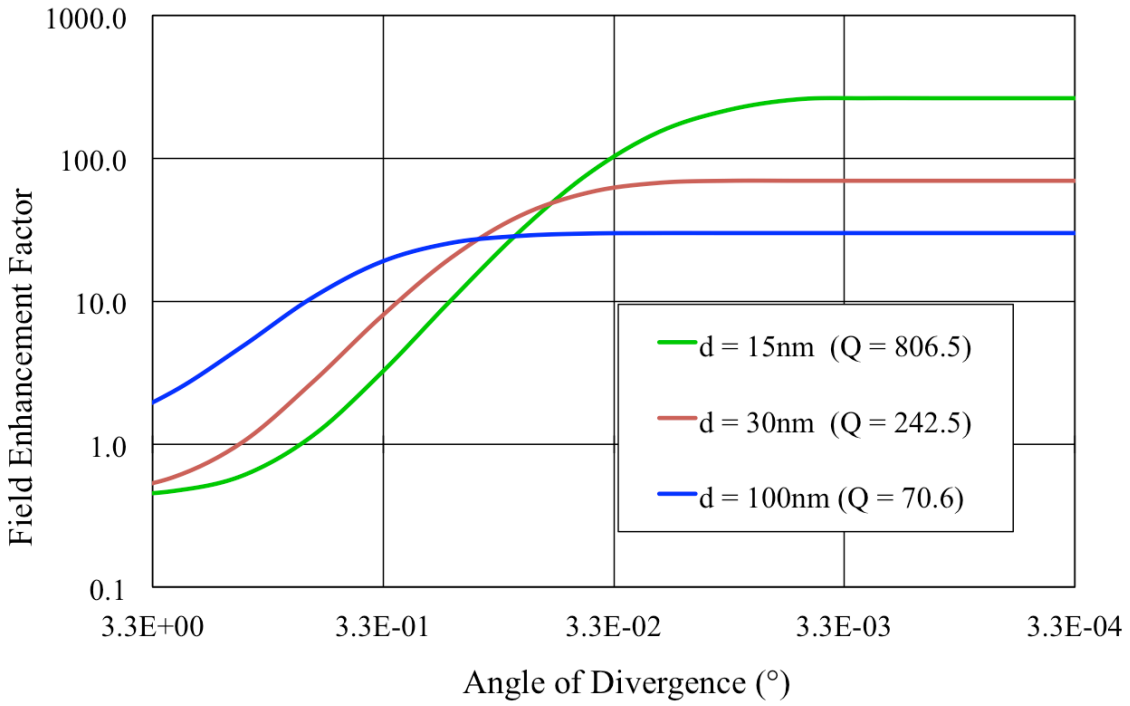

Figure 2.3 Simulated local field enhancement factor in terms of angle divergence of the excitation laser beam for PC substrates with different Q-factors.

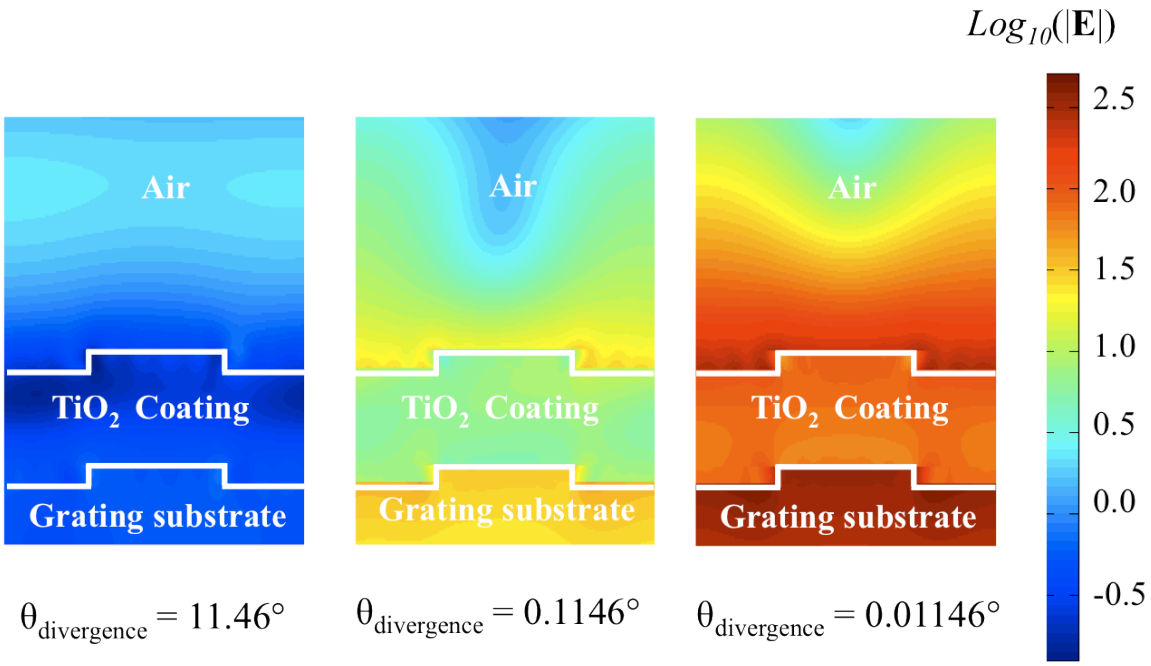

Figure 2.4 Simulated local field enhancement factor in terms of angle divergence of the excitation laser beam for PC surfaces with different angle of divergence for a 15 nm depth grating.

CHAPTER 3: ENHANCED FLUORESCENCE INSTRUMENTATION

Two different types of fluorescence detection systems were studied for PCEF: a commercially available microarray laser scanner and a modified fluorescence microscope that is specifically designed for PCEF.

The apparatus of the microarray laser scanner (LS Reloaded, Tecan Inc.) is shown in Figure 3.1(a). This system uses a focused laser beam (beam divergence ~ 2.5°) as the excitation source and a photomultiplier tube (PMT) as the fluorescence signal detector. In order to form an image, the substrate is scanned and the fluorescence signal intensity for each pixel is acquired. The apparatus of the custom-built fluorescent detection system, which is referred to as the PC enhanced fluorescence microscope (PCEFM), is shown in Figure 3.1(b). In the PCEFM system, the fluorescent sample is imaged by an electron-multiplying charge-coupled device (EMCCD, Hammamatsu Inc.) via a 4× microscope objective (numerical aperture N.A.= 0.1). Unlike the confocal laser scanner, the PCEFM works in the imaging mode, which significantly improves the measurement throughput. For both systems, a HeNe laser (λ = 632.8 nm) is used as an excitation light source, and a bandpass filter is placed in front of the detectors to reject excitation laser light.

The microarray laser scanner uses a lens with a high numerical aperture (NA) to focus the laser beam onto the sample and collects the fluorescence signal resulting from this excitation. Due to the focusing effect, the illumination laser beam angle spans from 0° to 30°. As a result, only a small portion of the excitation energy can be coupled into the resonant mode of the PC surface, thus compromising the enhancement performance of the PC. For the PC surface with $Q \approx 300$, the coupling efficiency is less than 20%. As discussed above, in order to take full

advantage of a PC and accomplish high enhancement of the fluorescence signal, it is critical to achieve a good coupling efficiency between the excitation laser beam and the PC surface. The PCEFM setup is designed specifically to achieve this and utilizes collimated illumination for this purpose. As shown in Figure 3.1(b), the output of the HeNe laser is expanded to produce a beam with diameter of 20 mm and divergence of 0.037° using a beam expander. In order to accurately control the angle of incidence, the PCEFM system utilizes a high-precision angle-tuning gimbal-mounted mirror that is itself mounted on a motorized linear stage that moves as the mirror rotates. The movement of this linear stage compensates for the beam shift due to incident angle variation and thereby ensures a fixed illumination area. The angle tuning resolution of this configuration is 0.005°, enabling one to test PC devices with angle bandwidth as narrow as 0.01°. A coupling efficiency of 98% has been achieved using this system with a PC surface with angle bandwidth of 0.3°.

3.1 Figure

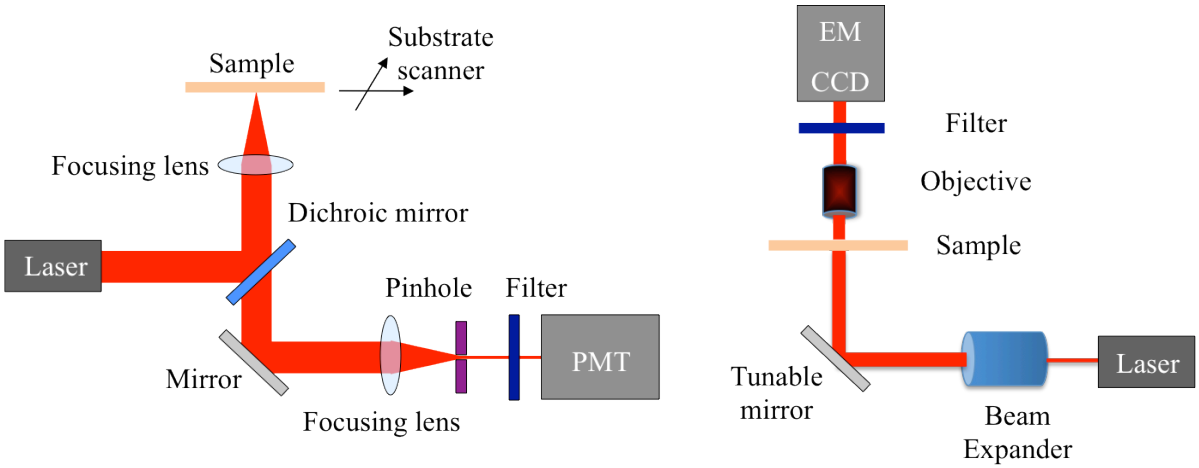

(a) Microarray laser scanner

(b) PC enhanced fluorescence microscope

Figure 3.1 (a) Schematic diagram of optical setup of the confocal laser scanner and (b) schematic drawing of PC enhanced fluorescence microscope.

CHAPTER 4: EXPERIMENTAL RESULTS

The PC sensor used in this work was fabricated using nano-imprint lithography (NIL) [34, 35]. The detailed fabrication procedure has been fully described in a previous publication [36]. The fabricated PC structure has a period of Λ=400 nm, duty cycle of 50%, and grating depth of d=40 nm. As a high index layer, 130 nm of TiO_2 was coated by RF-sputtering. Illuminated by a HeNe laser at λ=632.8 nm, this PC exhibits resonance at an angle of θ=10°. The coupling between the PC resonant mode and laser beam with different degrees of divergence was investigated. The enhancement capability of the PC was compared between the confocal laser scanner and the PCEFM.

4.1 Transmission Spectrum

In order to show the effect of laser beam divergence on the coupling between the PC and excitation light, we measured the transmission spectrum using focused and non-focused beams as illumination sources. To measure the transmission spectrum in terms of angle, the sample was illuminated by a He-Ne laser and the transmitted light power was monitored by a silicon photo-detector while the angle of incidence was scanned around the resonant angle (9.4° to 11.5°). Low transmission (high reflection) efficiency indicates good coupling of incident light into the resonant mode of the PC. The divergence of the incident laser beam was varied using lenses of different focal lengths. Without a focusing lens, the divergence angle is 0.057°; using lenses with focal lengths of 100 mm and 60 mm, the beam divergences are 0.45° and 0.76°, respectively. As shown in Figure 4.1, the measured transmission spectra were compared for the collimated and non-collimated illumination. Using a collimated laser beam, the transmission efficiency was 5%

at resonant angle with angle full width at half maximum of 0.37°. The transmission efficiency increases to 61% and 49% when the laser beam is focused by lenses with 100 mm and 60 mm focal lengths, respectively. Due to the broadening of incidence angle, a lower percentage of excitation energy is coupled into resonance, and transmission efficiency becomes higher. With regard to PC enhanced fluorescence, the diverged beam results in only a portion of the excitation energy being amplified by the PC resonance, which diminishes the fluorescence enhancement capability of the PC sensor.

4.2 Enhanced Fluorescence Intensity

Having established a clear relationship between degree of collimation of incident light and coupling efficiency with a PC, fluorescence measurements were performed to experimentally correlate the influence of degree of collimation of incident light with the extent of fluorescence enhancement. The microarray laser scanner and the PCEFM discussed in Chapter 3 were used, to represent cases for focused and collimated light. The signal enhancement factor for the on-resonance case with respect to the off-resonance case was measured over a range of angles around the resonance angle. This is shown in Figure 4.2.

The collimated light gave a signal enhancement factor almost 7x higher than the case for the focused light. This can be easily explained as a direct consequence of the higher magnitude of surface localized electric field intensity that interacts with fluorophores immobilized on the surface of the PC.

Another interesting observation was that the signal enhancement is much more sensitive to the proximity to the resonance angle for collimated excitation ($FWHM_{\theta} < 0.4°$) than for focused excitation (peak $FWHM_{\theta} > 1.5°$). This can be explained as a consequence of the sensitivity of the

coupling efficiency of the PC to change in excitation angle for collimated light. Thus, for the PCEFM a small deviation from the resonance condition will result in a large drop in the surface localized electric field intensity, ultimately leading to lower enhancement in fluorescence intensity. For the case of focused light, since the incident beam consists of a spread of angles, over a fairly large range there will always be some light present in the resonant angle range. Thus, even though the coupling will never be as efficient and the electric field intensities will never reach high values, the fluorescence enhancement will have a much greater angle tolerance. Thus the degree of collimation of the excitation light (which influences the coupling efficiency of the PC as described in the previous section) is the ultimate determining factor for the degree of enhancement. The sensitivity of the degree of enhancement to the proximity to the resonance angle has far-reaching implications for performing multiplexed assays on a PC surface.

We performed a study to analyze the total enhancement of the PC on-resonance compared to unpatterned glass. Figure 4.3 shows a bar graph plot for the signal enhancement as measured on the PCEFM and the confocal laser scanner. The plot shows a very high signal enhancement for the on-resonance case compared to the off-resonance case (169× for PCEFM, and 15× for the laser scanner), which is due to the enhanced excitation effect. The off-resonance case for the PC also has a higher signal as compared to a glass slide (~4× for the PCEFM and ~2× for the laser scanner). This is a result of the PC enhanced extraction effect [14]. In this case, emitted photons, which would ordinarily exit the surface distributed uniformly in all directions, are spatially biased away from the PC surface at an (approximately) normal angle, so they may be gathered more efficiently by the detection optics.

The combination of the two enhancement effects provides a net signal enhancement (compared to unpatterned glass) of ~677× using the PCEFM and ~29× using the laser scanner.

4.3 Angle-Scanned Image Optimization

Having established the superior performance of a PC under collimated conditions and the promise of high enhancement offered by the PCEFM, it is necessary to provide a uniform enhancement effect over substantial surface areas, such as those used for protein microarrays or DNA microarrays that are comprised of hundreds or thousands of capture spots. Because the enhancement factor is highly sensitive to the angle of incidence for a collimated beam (Figure 4.2), small variations in the PC surface resonant coupling angle caused by non-uniformities in the PC structure (for example, the TiO_2 layer thickness) and the density of surface functionalization layers will result in substantial variations in fluorescent intensity if a fixed incident angle is used to scan the entire device. This problem is further complicated by the variable density of immobilized capture molecules, such as DNA or antibodies, which are deposited as arrays of spots on the PC surface. Capture molecules are typically deposited with high density, and therefore result in a substantially lower PC coupling angle compared to the regions of the surface between capture spots. There is thus no single incident angle that can be used to optimally couple a laser to every region of a PC surface.

In order retain the benefits of signal enhancement while still performing fast, high-throughput measurements, we developed a methodology to account for the variation in the resonant coupling angle across the device. Rather than gathering fluorescent output images with the PCEFM using a single incident angle, we capture a sequence of fluorescence images over a range of angles that always includes the resonance angle. Software is used to compare the images taken at each angle, and to select the maximum intensity of every pixel over the scanning range. Because the maximum intensity for any pixel will always be generated when the incident angle

matches the optimal resonant condition, a new image can be constructed using the maximum intensity angle for each pixel.

To demonstrate the angle-scanning method, a 3×3 array of Poly(Lys, Phe) conjugated with Alexa-647 (Invitrogen) was spotted at a concentration of 9.9 μg/ml onto the 1×3 in^2 PC surface by a piezoelectric dispenser (Piezorray, Perkin Elmer) with a center-to-center separation of 500 μm and a spot radius of ~200 μm. Prior to spotting, the PC surface was pre-cleaned with O_2 plasma for 3 min and then cleaned by sonication in acetone, isopropanol and deionized (DI) water followed by drying under a nitrogen stream. After spotting, the PC was incubated for 24 hours in a sealed container. The spot densities were selected so as to give an approximate shift of -0.2° in the PC coupling condition.

Selecting a single incident angle of θ=10°, the PCEFM gathered the image shown in Figure 4.4a. Using a 4× microscope objective, a single fluorescent image has a field of view of ~2×2 mm^2. An automated motion stage enables capture of fluorescent images from adjacent regions, and concatenation of images results in a fluorescent image of the entire slide, using a total scanning time of 24 seconds. Nominally, each spot in the array is identical, but the fluorescent intensity shows the effects of nonoptimal laser coupling to the PC resonance in several regions of the chip, resulting in a coefficient of variability of CV=51% for the on-spot intensity.

Figure 4.4(b) is a fluorescence image of the same slide as in Figure 4.4(a) with the image constructed by the new methodology. For each imaged region, a sequence of fluorescence intensity images is gathered from 9.5°<θ<10.5° in 0.1° increments, for a total of 11 images per frame. By gathering the additional images, the scanning time for the entire 1x3 in^2 area increased to 48 sec. The maximum-pixel selection and composite image-processing algorithm runs in 60 sec. As a result of the new method, the spot CV is reduced to 17.9%. This level of

spot-to-spot variability is consistent with what is typically obtained for fluorescent images of spot intensities on glass surfaces (data not shown), and therefore represents variability due to the spots themselves, rather than variability in the detection method. Using the angle scanning approach, we observe a consistently high enhancement factor across the entire PC area.

4.4 Figures

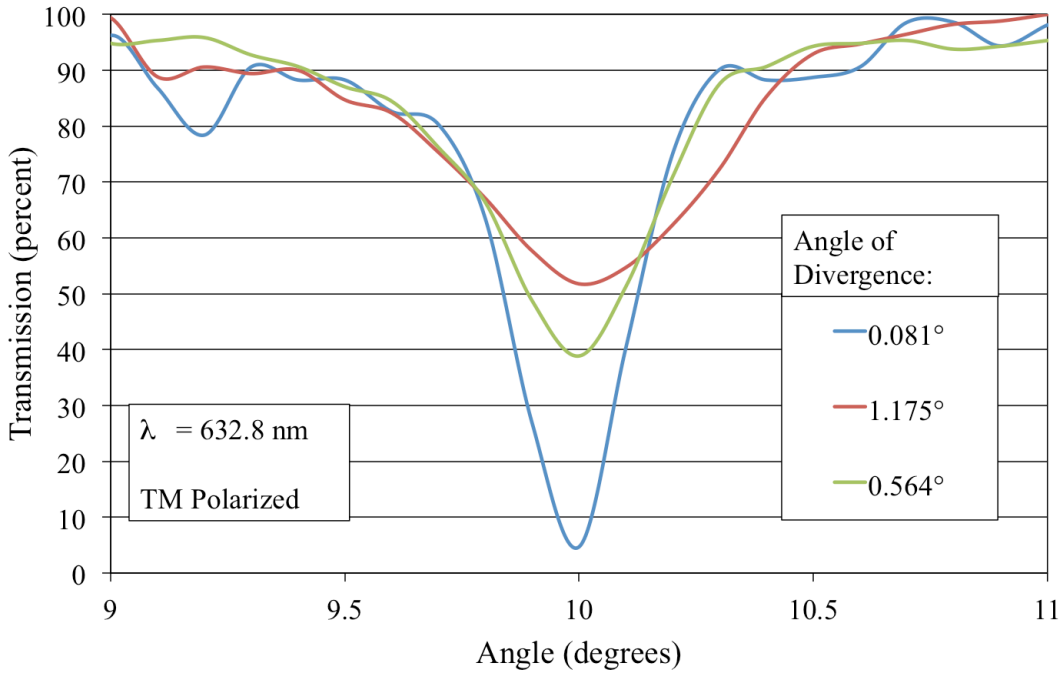

Figure 4.1 Transmission spectrum of a PC enhancement substrate where the resonant angle is around 10°. The illumination spot has divergence of 1.175°, 0.564°, and 0.081°.

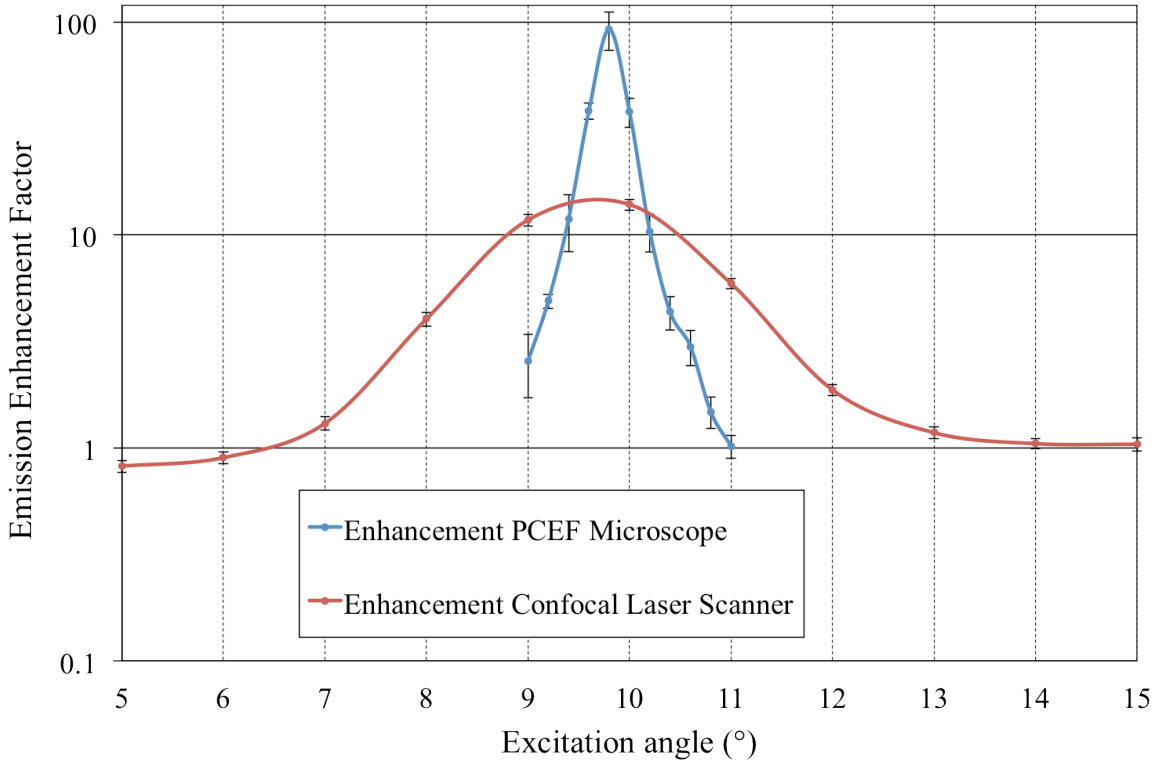

Figure 4.2 Comparison of the fluorescence intensity as a function of excitation angle measured using the PCEF microscope and the confocal laser scanner.

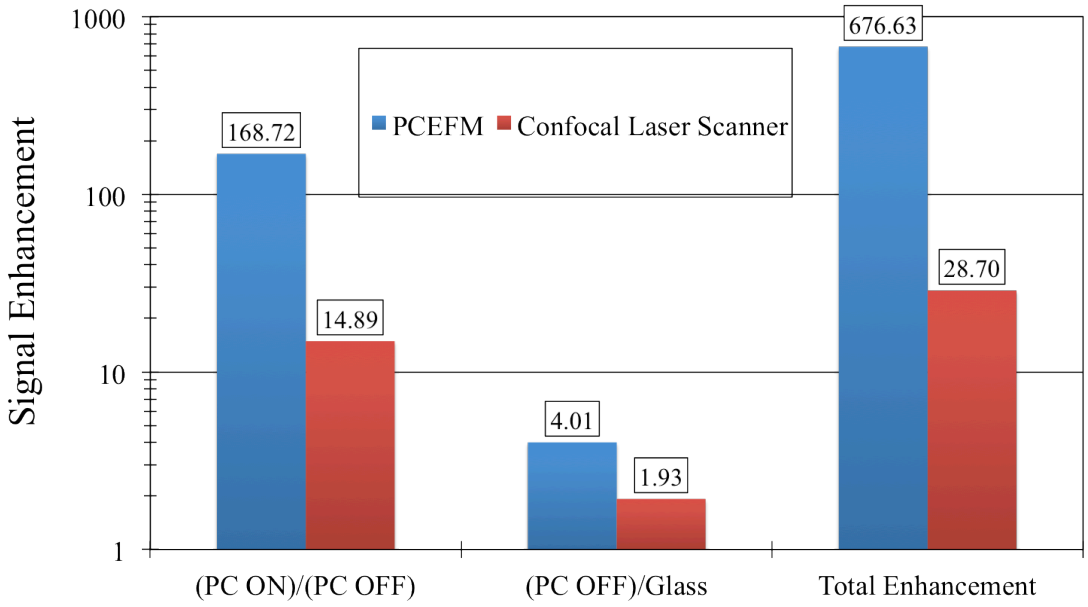

Figure 4.3 Comparison of the fluorescence enhancement using the PCEF microscope and the confocal laser scanner. The fluorescence signal enhancement for the PC on-resonance compared to the off-resonance case is attributed to the "enhanced excitation" property of the PC. The fluorescence signal enhancement for the PC off-resonance compared to unpatterned glass is attributed to the "enhanced extraction" property of the PC. The total enhancement is the ratio of the fluorescence signal for the PC on-resonance to the unpatterned glass.

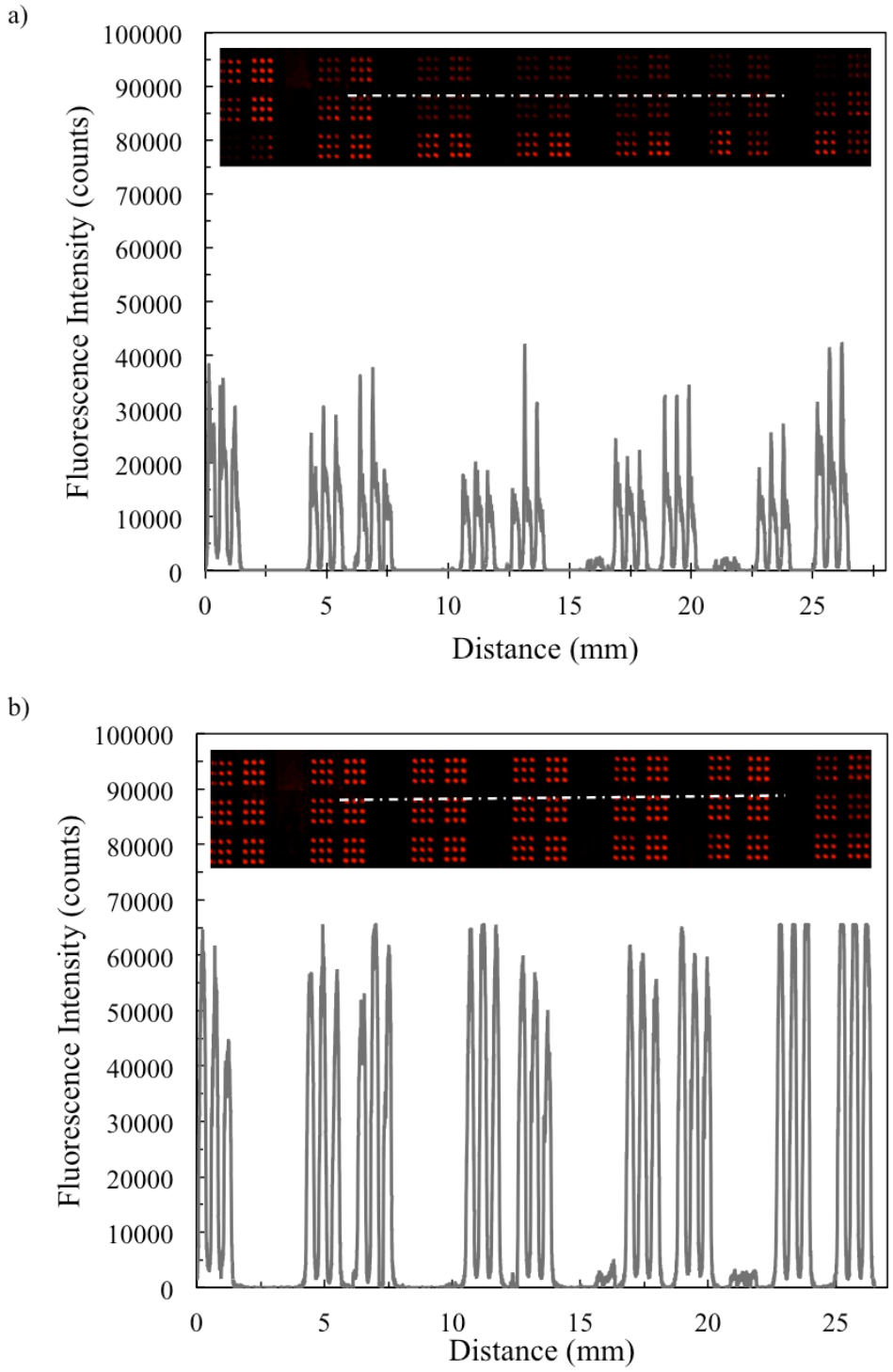

Figure 4.4 Intensity profile as a function of distance for a line of fluorescent image pixels profiling spots of Alexa-647 conjugated PPL for the PC (a) using a fixed excitation angle at 10° and (b) with the fluorescence intensity scanned at 11 angles near the resonance angle. The scanned images are shown in insets.

CHAPTER 5: PHOTOBLEACHING IN PHOTONIC CRYSTALS

5.1 Motivation

While PCEF has been applied to gene expression microarrays and protein biomarker detection [15], the relationship between fluorescence enhancement and the rate of photobleaching has not yet been characterized. Although photobleaching may not be of critical importance for single-measurement biomolecular assays, knowledge of photobleaching effects on PC surfaces will become important as researchers attempt to apply PCs to cell-based assays and single-molecule measurements of molecular machines using FRET (Forster Resonance Energy Transfer) probes [37]. The relationship between photobleaching and fluorescent enhancement factor is not completely straightforward for PCEF because only enhanced excitation is expected to participate in photobleaching, while the enhanced extraction effect is only redirecting emitted photons for more efficient collection. Further, the angle of incidence of a single wavelength collimated illumination source is extremely important in determining the degree of enhanced excitation of the resonant modes of the PC [7]. Therefore, the goal is to characterize the rate of photobleaching from a PC surface using a collimated illumination source and to study its dependence on the angle of illumination (and thus the extent of enhanced excitation). We study PCEF using a fluorescent microscope that incorporates a collimated monochromatic light source that can be precisely tuned to the resonant illumination angle to excite the PC resonance. This instrument enables us to match the illumination conditions (of incident wavelength and incident angle) to satisfy the resonant condition of the PC, so the illumination is called “on-resonance.” By adjusting the incident angle for a fixed wavelength so that the resonant coupling condition of the PC is not satisfied, the illumination may also be supplied in an “off-resonance” manner. We

observed that the photobleaching rate decreases substantially when off-resonance illumination is used, and that it is strongly correlated with the coupling efficiency between the PC and the illumination source, indicating that indeed only the enhanced excitation mechanism participates in modulating the photobleaching rate.

5.2 Photonic Crystal Configuration

In order to study photobleaching on substrates with fluorescence enhancement capability, a PC surface with periodic modulation in one direction was fabricated as shown in the cross-sectional diagram (not to scale) of Figure 5.1 (a). The surface grating structure was formed in an ultraviolet curable polymer (UVCP) on a polyethylene-terephthalate (PET) substrate, and the polymer grating surface was coated with a 300 nm SiO_2 spacer layer followed by a high refractive index dielectric layer of TiO_2, which functions as a wave confinement layer. In order to achieve a resonance at λ=632.8 nm, electromagnetics simulation software (DiffractMOD, RSoft Design Group) based on the rigorous coupled-wave analysis (RCWA) technique was used to design the PC, resulting in a desired grating period of 360 nm and grating depth d = 50 nm. Figure 5.1 (b) shows a top-down SEM image of a device fabricated to these design dimensions

Fabrication of the device was performed using a plastic-based nanoreplica molding process [17]. Briefly, a silicon wafer with a negative surface volume image of the desired grating pattern was fabricated using deep-UV lithography and reactive ion etching. A viscous liquid that contains an uncured monomer and a UV-activated polymerization initiator is sandwiched between a PET sheet and the silicon master wafer to enable the liquid to fill the silicon surface structure prior to curing with a high intensity UV lamp (Xenon, Inc). The hardened polymer grating preferentially adheres to the PET substrate, and thus can be easily peeled away from the

silicon. After the molding step, the replica was cut and attached to a 1 × 3 in^2 microscope slide. Using an e-beam evaporator (Denton Vacuum, Inc.), an intermediate SiO_2 layer (t_{SiO_2}= 300 nm) was deposited on the grating surface to reduce autofluorescence from the underlying polymer material due to dielectric sputtering. After the SiO_2 deposition, ~120 nm of TiO_2 was deposited by an RF sputtering system (PVD 75, Kurt Lesker) using an *in-situ* process monitor to accurately achieve a resonance condition that nominally results in λ=633 nm wavelength resonantly coupling to the PC surface at an incident angle of 2°. Figure 5.1 (c) shows the final device after all fabrications steps were completed.

For this study the PC was designed with a TM-polarized resonance close to the cyanine-5 (Cy5) excitation wavelength of λ=625 nm and a TE-polarized resonance spectrally overlapping the Cy5 emission spectrum centered at λ=690 nm. The TM resonance increases the excitation of the fluorophore through enhanced electric field intensities, while the TE resonance redirects a proportion of emitted light toward the detection instrumentation. Figure 5.2 (b) shows the transmission spectra of the PC measured using white light illumination at normal incidence, in which dips in the transmission spectra indicate a resonance.

5.3 Detection Instrumentation

The detection system used in the study is the same modified back-illuminated fluorescent microscope (Olympus BX51WI) described previously and shown schematically in Figure 3.1 (b). The microscope is equipped with a 4× objective (N.A. = 0.1) and an electron multiplying CCD (C9100-13 EM-CCD; Hammamatsu Inc.) for imaging. The EM-CCD provides control over the gain settings and integration times used during the imaging process. All results reported here were measured with a sensitivity gain of 161, an analog gain of 5 and an exposure time of

400 msec. A 35 mW, λ=632.8 nm HeNe laser was chosen as an excitation source that was aligned with the absorption spectrum of Cy5. A high-resolution, motorized, gimbal-mounted mirror and beam-expanded laser provide collimated illumination at a user-selectable incident angle to the PC. In order to maintain a constant illumination area on the device, the gimbal-mounted mirror sits on top of a motorized linear stage that moves as the mirror rotates. As the collimated light at a fixed wavelength is incident on the PC surface, the angle of incidence can be tuned to allow the laser to couple with the PC resonance, thereby allowing maximum field coupling into the TM mode of the PC. The excitation illumination was TM polarized by passing the laser light through a half-wave plate.

5.4 Methodology

A detection experiment using a Cy5-labeled protein was carried out on the PC surface and a reference glass slide in order to directly compare the rates of photobleaching. The PC surface and the glass slide were pre-cleaned with O_2 plasma for 5 min. Following the cleaning, both PC and glass were functionalized by overnight incubation in an enclosed glass container with 5% 3-glycidoxypropyldimethylethoxysilane in dry toluene at 100 °C. After incubation the silanized devices were cleaned by sonication in toluene, methanol and deionized (DI) water and then dried under a nitrogen stream. Cy5 conjugated streptavidin (GE Healthcare) at 10 μg/ml was spotted onto the slides by a piezo dispenser (Piezorray, Perkin Elmer) to produce 4x4 arrays of labeled protein spots of ~500 μm diameter. After overnight incubation, the devices were washed by gently dipping them in a protein blocking buffer (phosphate buffered saline at pH 7.4 with Kathon antimicrobial agent) solution for 60 sec followed by DI water rinse.

To perform measurements using the detection system in Figure 3.1 (b), the excitation laser was first tuned to the resonant angle without exposing the fluorophores. Next, a shutter was opened and 400 image frames were captured in sequence, exposing the sample each time for 400 msec. The shutter was closed and reopened before each measurement to avoid unnecessary exposure to light. All measurements were taken on the same sample from identical spots. In order to discern the effect of enhanced excitation on the photobleaching rate, data were recorded from the angles of maximum (on-resonance) and minimum (off-resonance) excitation, and from several intermediate angles. The transmission efficiency of the selected points is shown in Figure 5.2 (a). The selected angles are 20°, 2.46°, 2.23° and 2.03°, where the transmission efficiency of the PC is 100%, 76%, 52% and 26% (minimum transmission) respectively.

5.5 Results and Analysis

Figure 5.3 shows initial (first exposure) fluorescent images of streptavidin-Cy5 spots on the PC at 2.03° (on-resonance), 20° (off-resonance) and on the glass slide illuminated at 20°. The spots shown in Figure 5.3 clearly indicate enhanced excitation and enhanced extraction effects that also become evident upon analysis of the numerical data.

Figure 5.4 shows the fluorescent intensities collected for each angle over a period of 159 seconds. Each curve was measured at a different angle of excitation (and same excitation wavelength of λ=632.8 nm), starting with a fresh, unexposed array of spots. The output intensity on a set of 16 spots was recorded and averaged for each frame. The background value for each frame was then subtracted to give the final, average spot intensity. The final data are plotted on the same scale for comparison. The highest raw signal value is for the angle pertaining to the lowest transmission efficiency, corresponding to maximum resonant coupling of the excitation

laser with the PC surface. As expected, the curve corresponding to the 52% transmission (2.23°) has the next highest raw signal value, followed by the curve corresponding to 76% transmission (2.46°). Note that even when the PC is illuminated at an angle that is far from the resonant condition (20°), we still obtain greater signal output than with a glass surface. This high signal output is due to the enhanced extraction effect.

In order to compare the rates of photobleaching on the PC, each data set was normalized to the unpatterned glass control and each resulting curve fitted to an exponential function. The fitting equation used was as follows:

$$Signal\_Intensity = B \times e^{-At} \tag{5.1}$$

where A and B are fitting parameters indicative of the photobleaching decay rate and signal intensity gain.

Table 5.1 lists the values of parameters A and B for different excitation angles. We observe that, moving from the on-resonance case to the off-resonance case, there is a steady decrease in signal intensity gain and photobleaching decay rate. Thus for higher degrees of enhancement we see a greater rate of photobleaching. This trend can be attributed to the strength of the electric fields present close to the surface at various angles.

In order to investigate the effect more fully, we analyzed spatial plots of electric field intensity (close to the surface of the PC) obtained by rigorous coupled wave analysis (RCWA) electromagnetic field computer simulation (Rsoft, DiffractMod). Figure 5.5 shows cross sectional plots of the electric field at the four different angles of excitation. As expected from our detailed analysis in Chapter 2, we observe that the field intensity is also directly related to the degree of coupling with the resonant mode (highest field for the on-resonance case). The increase in the electric field intensity helps explain the reason for a higher enhancement and

subsequent higher rate of photobleaching. For a higher electric field intensity, more energy will be delivered to the fluorophores located near the surface, thus producing a higher fluorescence signal output.

It is important to note here that even though the rate of photobleaching is 30x higher for the PC on-resonance when compared to unpatterened glass (as indicated in Table 5.1), after hundreds of individual exposures, a 186x enhancement factor is still observed relative to measuring the same fluorophore on a glass surface after the final scan, compared to a 346x enhancement factor for the initial scan. In fact, in order to extrapolate to mathematically determine the exposure required to eliminate the benefits of the PC, we can equate the respective fitting equations (Eq. 5.1) for the PC on-resonance and glass cases:

$$B_{2.03^\circ} \times e^{A_{2.03^\circ} t} = B_{glass} \times e^{A_{glass} t} \tag{5.2}$$

$$346.71 \times e^{-0.0030t} = 1 \times e^{-0.0001t} \tag{5.3}$$

Inputting the respective values for constants A and B from Table 5.1 in the cases for the PC on-resonance and the glass, we find that for the fluorescence signal for the PC on-resonance to equal the fluorescence signal on the glass slide, both substrates would have to be subjected to constant exposure from the excitation laser for over 2000 seconds. Thus, for all practical experimental time frames, the fluorescence signal for the PC on-resonance will be higher than the fluorescence signal from an unpatterened glass substrate.

An interesting point to highlight here is that even though the signal intensity for the off-resonance case is 9x higher than that for the case of glass, the rate of photobleaching remains unchanged. This is a direct consequence of the extraction effect of a PC surface. The ability of the PC to allow emitted light to couple to a resonant mode and be directed towards the collection

lens allows for a high degree of enhancement of the signal without adversely affecting the rate of photobleaching.

5.6 Figures and Table

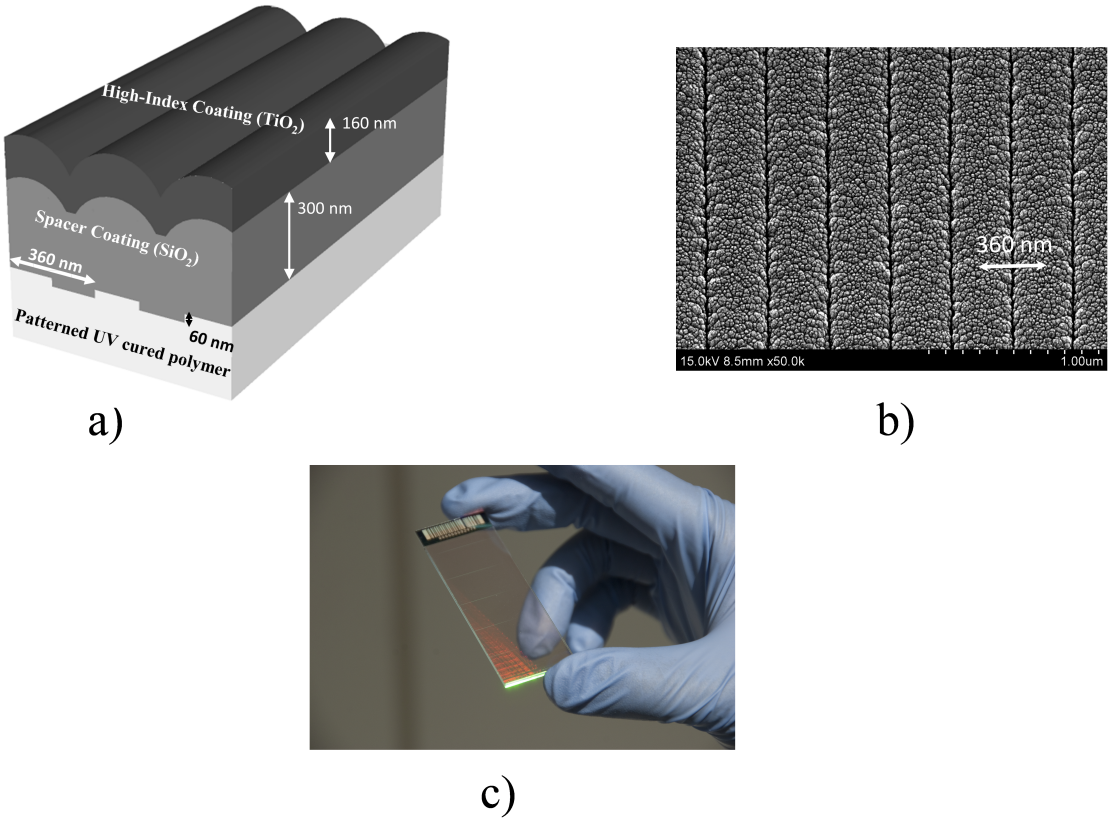

Figure 5.1 (a) Schematic cross sectional diagram of the photonic crystal structure. (b) Top view electron microscope image. (c) Photograph of the device attached to a standard glass microscope slide.

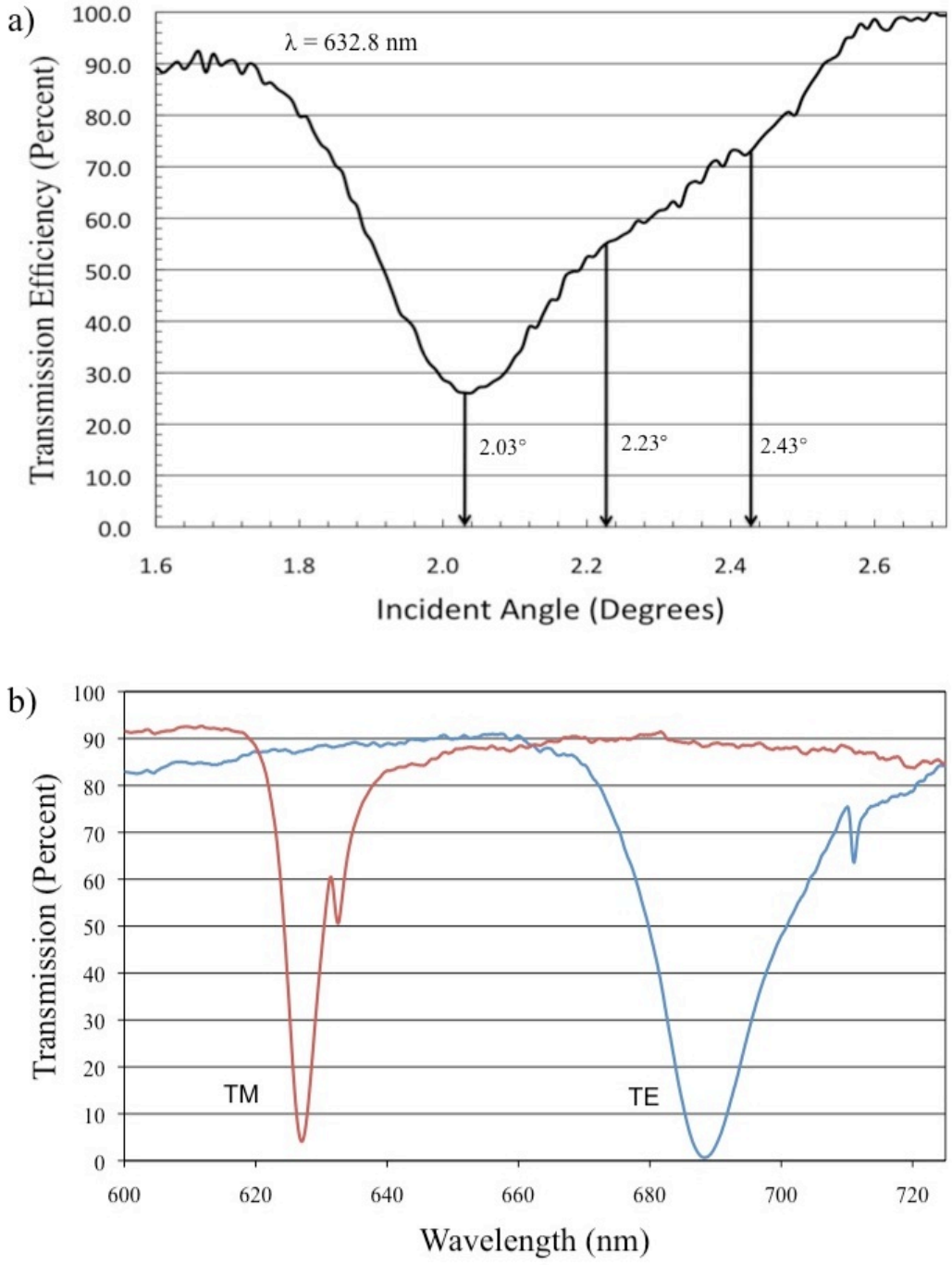

Figure 5.2 (a) Angular transmission spectrum for the transverse magnetic (TM) enhanced excitation mode showing the choice of various angles of excitation to generate optimal on-resonance excitation at an incident angle of 2.03°. (b) Transmission efficiency versus wavelength, showing dips in transmission intensity at normal incidence for the transverse electric (TE) (λ = 690 nm) and TM (λ = 625 nm) modes. Wavelengths of maximum resonance reflection correspond to wavelengths of minimum transmission.

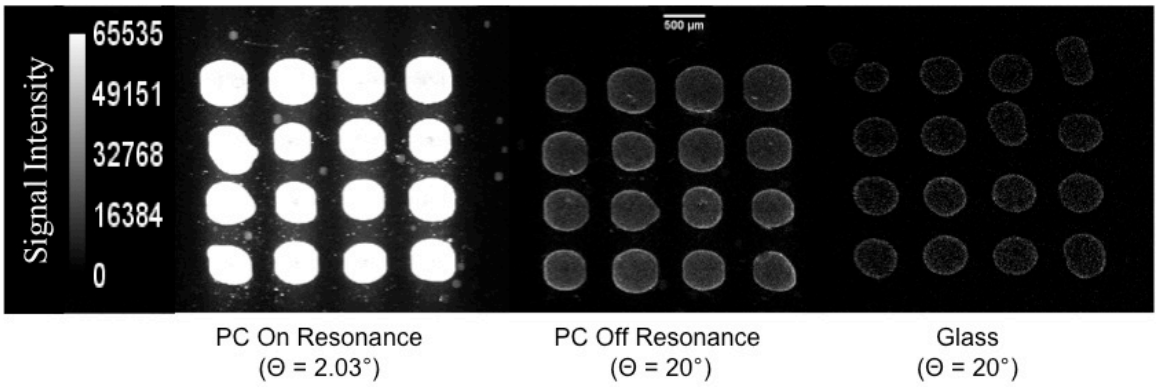

Figure 5.3 Images of Cy5-streptavidin spots taken for photonic crystal on-resonance (left), photonic crystal off-resonance (middle) and an unpatterned glass slide (right). Images were gathered with equal exposure and camera settings for direct comparison.

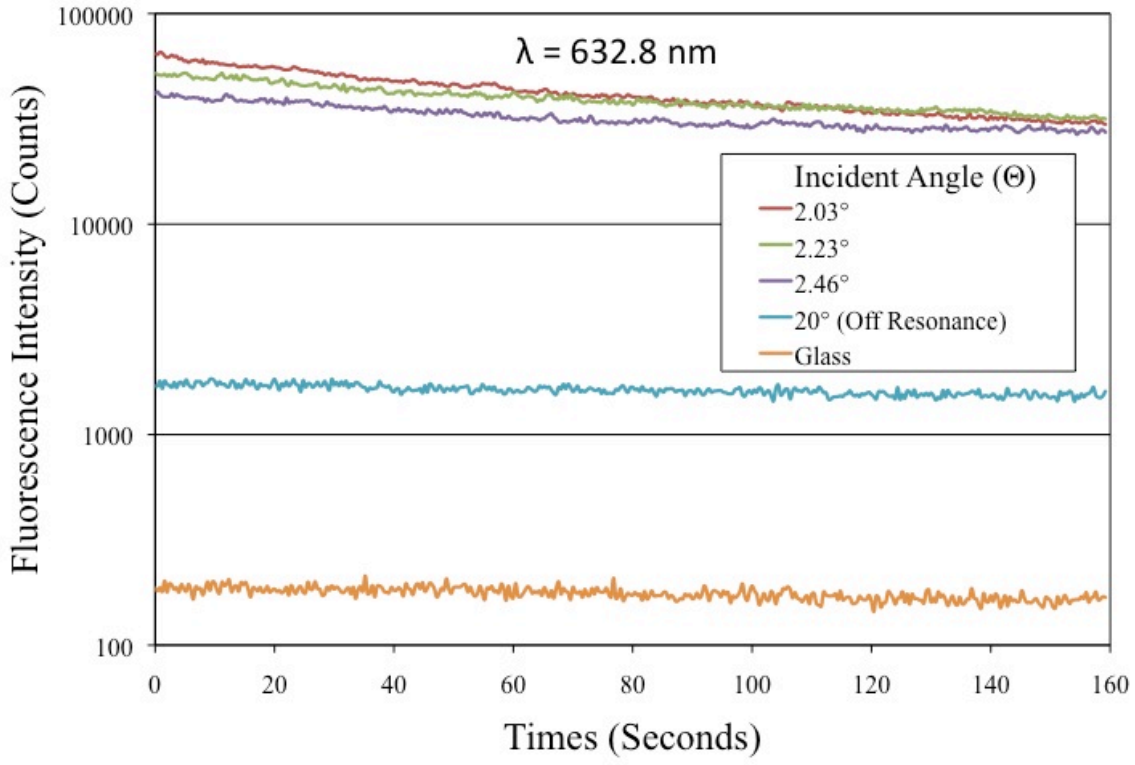

Figure 5.4 Plot of the measured fluorescence intensity versus time for continuous exposure at different angles of incidence for the excitation light.

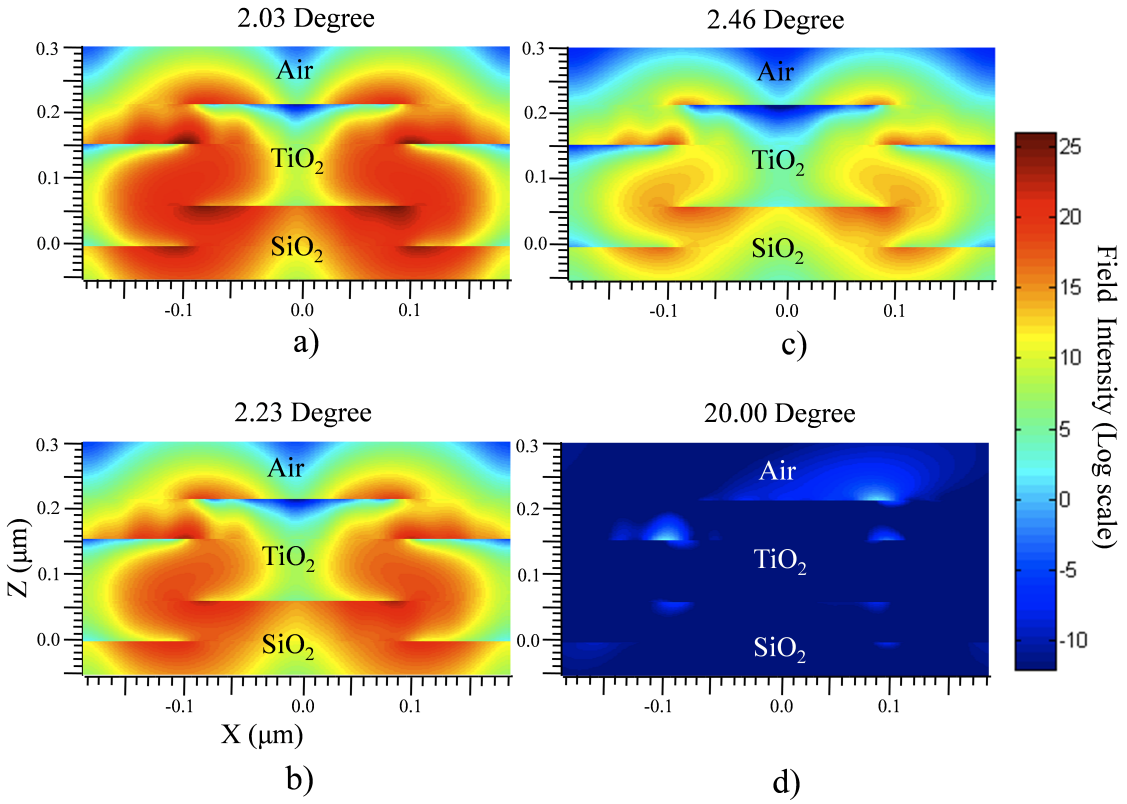

Figure 5.5 Electric field intensity plots generated using rigorous coupled wave analysis for excitation conditions corresponding to (a) 2.03°, (b) 2.23°, (c) 2.46° and (d) 20°. The electric field in the medium directly adjacent to the photonic crystal surface is modeled to be more than two orders of magnitude higher in the on-resonance (2.03°) condition, than in the off-resonance (20°) condition.

Table 5.1 Photobleaching decay rates and signal intensity gain as pertaining to excitation angle.

Device	**Angle of Excitation**	**Photobleaching decay rate ‘A’**	**Signal Intensity Gain ‘B’**
PC	2.03°	0.0030	346.71
PC	2.23°	0.0020	279.65
PC	2.46°	0.0010	223.40
PC	20.00°	0.0001	9.13
Glass	20.00°	0.0001	1

CHAPTER 6: CONCLUSION

This thesis has reported on the study of PC enhanced fluorescence illuminated with laser beams with different degrees of divergence. By use of an imaging system that enables angle-tunable collimated illumination of the PC surface, we have established improved performance for PCs when subjected to collimated excitation as compared to focused excitation in a confocal laser scanner, demonstrating raw signal enhancement of 677x. The signal enhancement is accompanied by an extreme sensitivity to the angle of excitation. This results in a problem of variability when attempting to utilize the PCEFM for high throughput measurements, such as those used in DNA microarrays or protein microarrays. In order to address this issue, an angle-scanning method was developed that allows optimal coupling to every pixel in a PC-based fluorescent image, and thus achieves a uniformly high enhancement factor over large surface areas. Finally, we correlated the rate of fluorescent photobleaching in the PC with the level of resonant fluorescent enhancement. Accelerated fluorescent photobleaching rates in a resonantly excited PC are a direct consequence of the enhancement of the surface localized electric fields exposed to adsorbed fluorescent dye molecules. We showed that, while the mechanism of enhanced excitation for PCEF accelerates photobleaching in proportion to the coupling efficiency of the laser to the photonic crystal in the context of the angle scanning technique that has been presented in this study, this accelerated photobleaching rate has a nominal effect on the fluorescence signal output owing to the time scale over which the angle scanning measurements are taken.

Therefore, PCEF optimized by excitation laser scanning is a viable tool in addressing device non-uniformity issues that can influence the efficacy and reliability of a PC in the context of large area microarray experiments. In the near future, the author hopes to combine this technique

with the ability of the PC to perform label-free scans to identify microarray spots and produce selective enhancement of microarray spots over background, thus lowering the detection threshold in microarray experiments.

REFERENCES

[1] J. W. Lichtman and J.-A. Conchello, "Fluorescence microscopy," *Nature Methods,* vol. 2, p. 910, 2005.

[2] J. Stenken, "Introduction to fluorescence sensing," *Journal of the American Chemical Society,* vol. 131, p. 10791, 2009.

[3] W. Budach, D. Neuschaefer, C. Wanke, and S.-D. Chibout, "Generation of transducers for fluorescence-based microarrays with enhanced sensitivity and their application for gene expression profiling," *Analytical Chemistry,* vol. 75, pp. 2571-2577, 2003.

[4] H. Jin and R. C. Zangar, "Protein modifications as potential biomarkers in breast cancer," *Biomarker Insights,* vol. 4, pp. 191-200, 2009.

[5] P. C. Mathias, H.-Y. Wu, and B. T. Cunningham, "Employing two distinct photonic crystal resonances for improved fluorescence enhancement," *Applied Physics Letters,* vol. 95, pp. 21111-21113, 2009.

[6] N. Ganesh, I. D. Block, P. C. Mathias, W. Zhang, V. Malyarchuk, and B. T. Cunningham, "Leaky-mode assisted fluorescence extraction: Application to fluorescence enhancement biosensors," *Optics Express,* vol. 16, pp. 21626-21640, 2008.

[7] I. D. Block et al, "A detection instrument for enhanced-fluorescence and label-free imaging on photonic crystal surfaces," *Optics Express,* vol. 17, pp. 13222-13235, 2009.

[8] H. Y. Wu, W. Zhang, P. C. Mathias, and B. T. Cunningham, "Magnification of photonic crystal fluorescence enhancement via TM resonance excitation and TE resonance extraction on a dielectric nanorod surface," *Nanotechnology,* vol. 21, pp. 125-203, Mar. 2010.

[9] W. A. Challener, J. D. Edwards, R. W. McGowan, J. Skorjanec, and Z. Yang, "A multilayer grating-based evanescent wave sensing technique," *Sensors and Actuators B: Chemical,* vol. 71, pp. 42-46, 2000.

[10] D. Rosenblatt, A. Sharon, and A. A. Friesem, "Resonant grating waveguide structures," *IEEE Journal of Quantum Electronics,* vol. 33, pp. 2038-2059, Nov. 1997.

[11] Y. Ohtera, T. Onuki, Y. Inoue, and S. Kawakami, "Multichannel photonic crystal wavelength filter array for near-infrared wavelengths," *Journal of Lightwave Technology,* vol. 25, pp. 499-503, Feb. 2007.

[12] D. Dobbs and B. T. Cunningham, "Optically tunable photonic crystal reflectance filter," *Applied Optics,* vol. 45, pp. 7286-7293, 2006.

[13] E. M. Purcell, "Spontaneous emission probabilities at radio frequencies," *Physical Review,* vol. 69, pp. 681-681, 1946.

[14] N. Ganesh et al., "Leaky-mode assisted fluorescence extraction: Application to fluorescence enhancement biosensors," *Optics Express,* vol. 16, pp. 21626-21640, 2008.

[15] P. C. Mathias, N. Ganesh, and B. T. Cunningham, "Application of photonic crystal enhanced fluorescence to a cytokine immunoassay," *Analytical Chemistry,* vol. 80, pp. 9013-9020, 2008.

[16] B. T. Cunningham, B. Lin, J. Qiu, P. Li, J. Pepper, and B. Hugh, "A plastic colorimetric resonant optical biosensor for multiparallel detection of label-free biochemical interactions," *Sensors and Actuators B,* vol. 85, pp. 219-226, 2002.

[17] I. D. Block, L. L. Chan, and B. T. Cunningham, "Photonic crystal optical biosensor incorporating structured low-index porous dielectric, " *Sensors and Actuators B,* vol. 120, pp. 187-193, December 14, 2006.

[18] B. T. Cunningham et al., "Label-free assays on the BIND system," *Journal of Biomolecular Screening,* vol. 9, pp. 481-490, 2004.

[19] B. T. Cunningham and L. L. Laing, "Label-free detection of biomolecular interactions: Applications in proteomics and drug discovery," *Expert Reviews in Proteomics,* vol. 3, pp. 271-281, 2006.

[20] L. Chan, S. Gosangari, K. Watkin, and B. T. Cunningham, "A label-free photonic crystal biosensor imaging method for detection of cancer cell cytotoxicity and proliferation," *Apoptosis,* vol. 12, pp. 1061-1068, 2007.

[21] L. L. Chan, S. Gosangari, K. L. Watkin, and B. T. Cunningham, "Label-free imaging of cancer cells using photonic crystal biosensors and application to cytotoxicity screening of a natural compound library," *Sensors and Actuators B,* vol. 132, pp. 418-425, 2008.

[22] L. L. Chan, P. Y. Li, D. Puff, and B. T. Cunningham, "A self-referencing method for microplate label-free photonic crystal biosensors," *IEEE Sensors,* vol. 6, pp. 1551-1556, 2006.

[23] L. L. Chan, M. F. Pineda, J. Heeres, P. Hergenrother, and B. T. Cunningham, "General method for discovering inhibitors of protein-DNA interactions using photonic crystal biosensors," *ACS Chemical Biology,* vol. 3, pp. 437-448, 2008.

[24] P. Li, B. Lin, J. Gerstenmaier, and B. T. Cunningham, "A new method for label-free imaging of biomolecular interactions," *Sensors and Actuators B, Chemical,* vol. 99, pp. 6-13, 2004.

[25] N. Ganesh, P. C. Mathias, W. Zhang, and B. T. Cunningham, "Distance dependence of fluorescence enhancement from photonic crystal surfaces," *Journal of Applied Physics,* vol. 103, p. 083104, 2008.

[26] P. Kramper et al., "Direct spectroscopy of a deep two-dimensional photonic crystal microresonator," *Physical Review B,* vol. 64, p. 233102, 2001.

[27] C. J. Barrelet, J. M. Bao, M. Loncar, H. G. Park, F. Capasso, and C. M. Lieber, "Hybrid single-nanowire photonic crystal and microresonator structures," *Nano Letters,* vol. 6, pp. 11-15, Jan. 2006.

[28] P. C. Mathias, N. Ganesh, W. Zhang, and B. T. Cunningham, "Graded wavelength one-dimensional photonic crystal reveals spectral characteristics of enhanced fluorescence," *Journal of Applied Physics,* vol. 103, p. 094320, 2008.

[29] I. D. Block, N. Ganesh, M. Lu, and B. T. Cunningham, "A sensitivity model for predicting photonic cyrstal biosensor performance," *IEEE Sensors,* vol. 8, pp. 274-280, 2008.

[30] K. J. Halbhuber and K. Konig, "Modern laser scanning microscopy in biology, biotechnology and medicine," *Annals of Anatomy-Anatomischer Anzeiger,* vol. 185, pp. 1-20, Jan. 2003.

[31] W. B. Amos and J. G. White, "How the confocal laser scanning microscope entered biological research," *Biology of the Cell,* vol. 95, pp. 335-342, 2003.

[32] S. Paddock, "Over the rainbow: 25 Years of confocal imaging," *BioTechniques,* vol. 44, pp. 643-648, 2008.

[33] B. E. A. Saleh and M. C. Teich, *Fundamentals of Photonics*, 1st ed. vol. 3. Boston, MA: Wiley, 1991.

[34] S. Y. Chou, P. R. Krauss, and P. J. Renstrom, "Imprint of sub-25 nm vias and trenches in polymers," *Applied Physics Letters,* vol. 67, pp. 3114-3116, 1995.

[35] S. Y. Chou, P. R. Krauss, and P. J. Renstrom, "Imprint lithography with 25-nanometer resolution," *Science,* vol. 272, pp. 85-87, April 5, 1996.

[36] A. Pokhriyal, M. Lu, V. Chaudhery, C.-S. Huang, S. Schulz, and B. T. Cunningham, "Photonic crystal enhanced fluorescence using a quartz substrate to reduce limits of detection," *Optics Express,* vol. 18, pp. 24793-24808, 2010.

[37] R. Roy, S. Hohng, and T. Ha, "A practical guide to single-molecule FRET," *Nature Methods,* vol. 5, pp. 507-516, Jun. 2008.